J. Math. Computer Sci., 42 (2026), 43–63

Online: ISSN 2008-949X

Journal of Mathematics and Computer Science

Journal Homepage: www.isr-publications.com/jmcs

Mathematical modeling of Nipah virus disease with optimal intervention strategies

A. Karthik, Mini Ghosh*

Department of Mathematics, School of Advanced Sciences, Vellore Institute of Technology, Chennai 600127, India.

Abstract

Since 1998, the Nipah virus disease, a deadly zoonotic disease that affects both humans and nonhuman primates, has erupted numerous times in various areas. In this study, we develop a Nipah virus (NiV) transmission model to explore how the Nipah virus spreads through both direct and indirect transmission from bats to humans and among human populations. The main objective of this study is to assess the impact of hospitalization protocols and control measures on minimizing infection within the human population. After calculating the equilibrium points and the basic reproduction number, we look at the local stability of the equilibrium points. We perform sensitivity analysis to scrutinize the impact of the model parameters on the basic reproduction number. Finally, this study extends to incorporate optimal control theory. Proposed control strategies encompass the culling of bats, reduction of human-to-human transmission, and augmentation of treatment protocols and testing infrastructure. Implementing these control measures results in a significant decrease in disease propagation.

Keywords: Nipah virus, mathematical model, stability, sensitivity analysis, optimal control, cost-effectiveness analysis.

2020 MSC: 34D20, 65C30, 92C50.

1. Introduction

Nipah virus (NiV) is a zoonotic pathogen transmitted from animals like bats and pigs to humans; these animals can contaminate food with saliva secretion and metabolic waste substances expelled from the body of the infected animals. Once bats are infected, they remain diseased for the rest of their lives. Additionally, humans can also directly transmit this virus to other humans. Figure 1 displays outbreaks of NiV in Southeast Asian countries such as Malaysia, Singapore, Bangladesh, and India. The first documented outbreak occurred in Malaysia in 1998, resulting in 283 reported cases and a mortality rate of 39% (109 deaths). The virus subsequently moved to Singapore and Bangladesh, with other outbreaks occurring in India in Siliguri in 2001, Noida in 2007, and Kerala in 2018 and 2023. The case mortality rate in Bangladesh was 73%, 72% in India, and 37% in Malaysia and Singapore. Overall, the fatality rate for the Nipah virus is 60%. The designation NiV traces its origins to the village of 'Kampung Sungai Nipah' in Malaysia, where its first identification occurred amid an outbreak. The initial investigation of the Nipah virus utilized diagnostic tests. Pteropid fruit bats, which consume the sap, may occasionally contaminate

*Corresponding author
Email addresses: karthik.2021a@vitstudent.ac.in (A. Karthik), minighosh@vit.ac.in (Mini Ghosh)

doi: 10.22436/jmcs.042.01.03

Received: 2025-04-02 *Revised:* 2025-06-29 *Accepted:* 2025-09-18

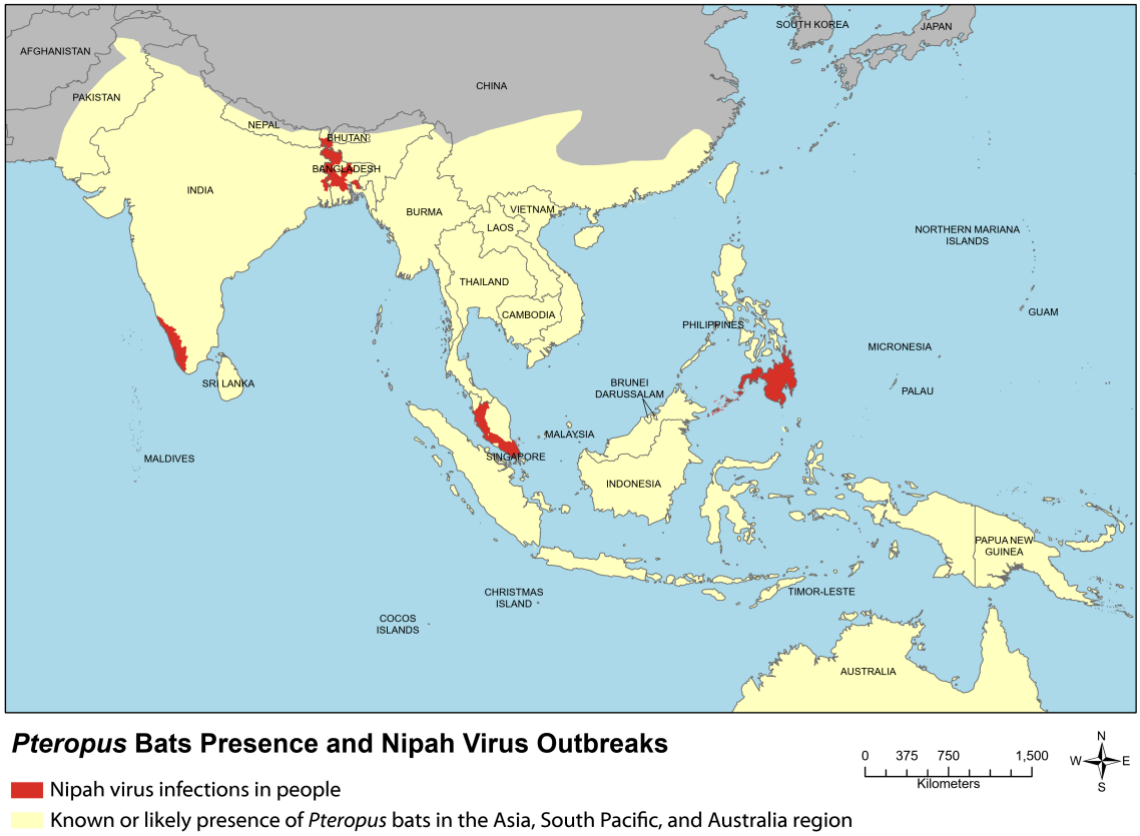

Figure 1: Illustrates outbreaks of the Nipah virus (source: [10])

the contents of the sap collection pot with urine or feces. Consequently, humans may become infected with the Nipah virus by consuming contaminated raw date palm sap. Molasses is produced by cooking sap at a temperature high enough to kill the Nipah virus. The first outbreak in Malaysia mostly impacted pig farmers, who contracted the virus from sick pigs. To contain the spread, 900,000 pigs were culled. [36] Most individuals have symptoms of the Nipah virus, such as fever, headache, dizziness, vomiting, and advancing to a comatose state, which typically manifests within 24 to 48 hours. It can lead to Encephalitis or respiratory infections for both animals and humans, ultimately resulting in death. Nipah virus currently has no vaccine or specialized treatment available [40]. The treatment for the Nipah virus involves supportive care, such as rest, hydration, and addressing symptoms as they arise. It is widely accepted within scientific discourse that the incubation period typically ranges from 4 to 14 days. However, there exist documented cases where the incubation period has extended up to 45 days [39].

In [35], authors investigated the effectiveness of two distinct control measures: increased awareness to reduce NiV transmission and enhanced treatment measures to decrease the number of infected individuals. In [27], authors suggested that implementing quarantine measures and emphasizing enhanced personal hygiene practices could potentially mitigate the spread of the NiV. In [32], authors explored the transmission dynamics of the NiV by utilizing the SEI model and assessed the stability of model equilibria both locally and globally. To assess the influence of vaccination on both disease prevention and recovery, the authors of [34] formulated and analyzed the NiV model for both animal and human populations by incorporating vaccination scenarios as well as non-vaccination scenarios. In [41], the authors formulated an SIRD model based on the hypothesis that deceased individuals might play a role in disease transmission. Their findings indicate that implementing interventions to minimize unprotected contact and expedite the removal of deceased bodies from infected individuals could result in a reduction of the basic reproduction number (R_0) below one, thereby facilitating the containment of the Nipah outbreak. In [28], the authors assessed the impact of treatment class on the spreading of the NiV and

proposed three control strategies for controlling its spread. The authors of [26] created and examined a model called SEITR to study how NiV spreads and how to control it. By employing the RK-45 method, they investigated the effect of disease parameters on the disease dynamics. In [42], authors proposed a mathematical model by incorporating human, bat, and animal populations to illustrate the transmission dynamics of the virus. This study involved analyzing four equilibrium points and implementing three control mechanisms. While protective gear cannot entirely prevent infection, it contributes significantly to mitigating human disease. In [8] authors proposed a mathematical model that incorporates human, bat, and pig populations to examine the stability of various equilibrium points. The consumption of food items contaminated with bodily fluids, saliva, or urine from infected animals, such as fruits contaminated by an infected bat, represents a notable threat to human health [10]. The study [2] aimed to evaluate the early diagnosis and treatment of the cholera virus through the implementation of remedial methods, both with and without pharmacological interventions. In [3] authors examined the transmission of SARS-CoV-2 (SC-2) and its impact on heart attack occurrences in the UK through a fractional-order mathematical model. This study investigated stability, bifurcation, and global effects, utilizing simulations to illustrate their collective impact on patients with heart conditions. In [5], authors examined COVID-19 transmission by incorporating both symptomatic and asymptomatic cases through a fractional-order mathematical model. The findings contribute to early detection, comprehension of outbreaks, and the formulation of future control strategies. In [1], the authors employed a fractional-order approach to model the transmission dynamics of the Nipah virus by incorporating the impact of waiting distribution.

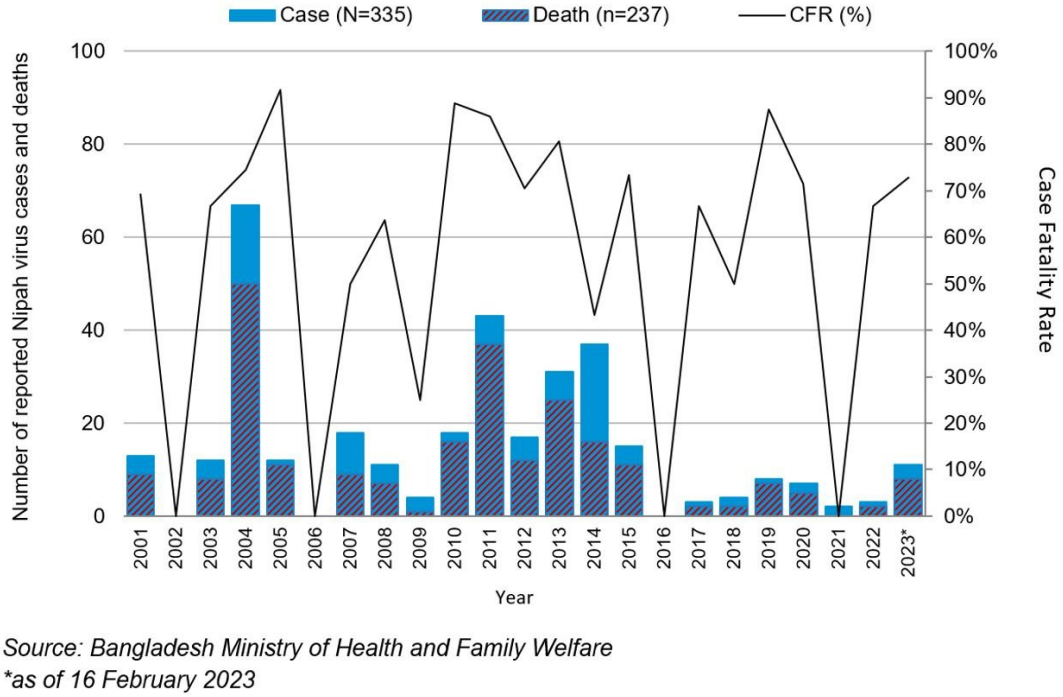

Figure 2: Annual count of Bangladesh's Nipah virus infections and fatalities.

In [16], the authors developed a mathematical model that employs a differential operator with the Mittag-Leffler function to explore the transmission dynamics of the Nipah virus, aiming to accurately depict the exponential and power laws often observed in natural phenomena. In [31], the authors developed and examined a mathematical model for Nipah virus regulated by fractional-order differential equations, encompassing two transmission modes of the disease: food-borne and human-to-human. Subsequently, they expanded this model to a fractional optimal control model to determine the most cost-effective control strategy for mitigating the disease's transmission. The study [7] indicated that exposure to an infectious deceased corpse could also result in an elevated spread of the Nipah virus. They developed an SIRD model and conducted a numerical investigation utilizing the Adams-Bashforth-Moulton ap-

proach. The study [4] develops a fractional-order mathematical model for the transmission of pine wilt disease, incorporating control and asymptomatic variables. Stability, bifurcation, and sensitivity analyses are performed, with numerical simulations demonstrating disease spread and control effectiveness. The authors of [14] employed fractional derivatives in the Caputo sense to investigate the nature of the Nipah virus. In [21], the authors examined the optimal control analysis of Nipah virus infection, using time-dependent treatment and vaccine strategies based on actual data from Bangladesh. In this research endeavor, an eight-compartment epidemiological model is being developed for the Nipah virus to examine various pathways by which individuals may contract infectious diseases. These pathways include indirect transmission via interactions between bats and humans, and direct transmission from human to human. Additionally, the model integrates hospitalized compartments and optimal control strategies.

The infected bat population and contaminated food spread the Nipah virus. Fruit bats are primarily cause Nipah outbreaks by contaminating date palm sap, followed by human-to-human transmission. The virus may also increase transmission, but most prior studies don't include the virus compartment. Some articles include the virus compartment, but they do not address hospitalization or treatment such as [1, 21, 25, 29, 31]. Hospitalization is important for the Nipah virus because without proper treatment, severe cases progress to coma within 24 to 48 hours. The need for such a comprehensive framework motivates this study.

This study introduces a novel mathematical modeling framework that includes compartments for both exposed and hospitalized individuals within human populations. In addition, a separate compartment for the virus population is considered, since it can survive for a few days in the environment. The study presents data fitting for Bangladesh from 2001 to 2015. While our model analyzes stability, fits data for Bangladesh from 2010 to 2023, and forecasts trends from 2024 to 2027 using the maximum likelihood estimation, we also compute the 95% confidence intervals for the estimated parameters to quantify uncertainty and ensure robustness of the predictions. Additionally, the model applies various optimal control strategies to mitigate the spread of disease.

The subsequent sections of this study are structured as follows. Section 2 pertains to model formulation. Section 3 calculates equilibria, the basic reproduction number (R_0), and conducts sensitivity analysis. Section 4 is dedicated to numerical simulation, demonstrating the effects of parameter variations-subsequently, Section 5 delves into an extensive discussion of the optimal control problem and its simulation. The study ultimately concludes in Section 6 with a concise discussion and conclusion.

Figure 2 depicts the annual count of Bangladesh's Nipah virus infections and fatalities. Typically, the Nipah virus has demonstrated a pattern of seasonal outbreaks between December and May, corresponding with the harvesting season of date palm sap (DPS).

2. Model formulation

This research study involves developing and analysing an eight-compartment epidemiological model for the Nipah virus. The NiV is transmitted from bats to humans and can also spread from human to human. The method entails dividing bat and human populations into eight separate compartments, namely: Virus (V), Susceptible bat (S_b), Infected bat (I_b), Susceptible human (S_h), Exposed human (E_h), Infected human (I_h), Hospitalization (H), and Recovered (R).

The schematic flow diagram of our model is depicted in Figure 3, where the solid lines symbolize an individual transitioning from one compartment to another and dotted lines symbolize the interaction of individuals across compartments. Building upon these assumptions, we develop the following mathematical model.

1. In this model, the virus-shedding rate of an infected bat is represented by the variable ρ, while the decay rate is denoted by θ.
2. The constant rate Λ_h and Λ_b signifies the recruitment of individuals into the susceptible human class and susceptible bat class within a specified region, respectively.
3. When susceptible bats come into contact with the virus, they become infected at a rate β_1.

4. When susceptible humans are directly exposed to a virus, they transition to exposed humans at a rate of β_2. Likewise, when a susceptible human interacts with an infected human, they become exposed humans at a rate of β_3.
5. Here η denotes the rate at which exposed human individuals progress to the infected human compartment.
6. The rate at which individuals move from the infected compartment to the hospitalized compartment is given by ϵ which denotes the hospitalization rate. Similarly, the recovery rate is given by α which corresponds to the movement of individuals from the hospital to the recovered compartment after recovery.
7. μ and μ_b are the natural death rates for the human and bat populations, respectively.
8. δ and κ are the disease-related death rates for the infected human population and hospitalized populations, respectively.

$$\begin{aligned}
\frac{dV}{dt} &= \rho I_b - \theta V, & \frac{dS_b}{dt} &= \Lambda_b - \beta_1 V S_b - \mu_b S_b,\\
\frac{dI_b}{dt} &= \beta_1 V S_b - \mu_b I_b, & \frac{dS_h}{dt} &= \Lambda_h - (\beta_2 V + \beta_3 I_h) S_h - \mu S_h,\\
\frac{dE_h}{dt} &= (\beta_2 V + \beta_3 I_h) S_h - (\eta + \mu) E_h, & \frac{dI_h}{dt} &= \eta E_h - (\delta + \mu + \epsilon) I_h,\\
\frac{dH}{dt} &= \epsilon I_h - (\mu + \alpha + \kappa) H, & \frac{dR}{dt} &= \alpha H - \mu R.
\end{aligned} \tag{2.1}$$

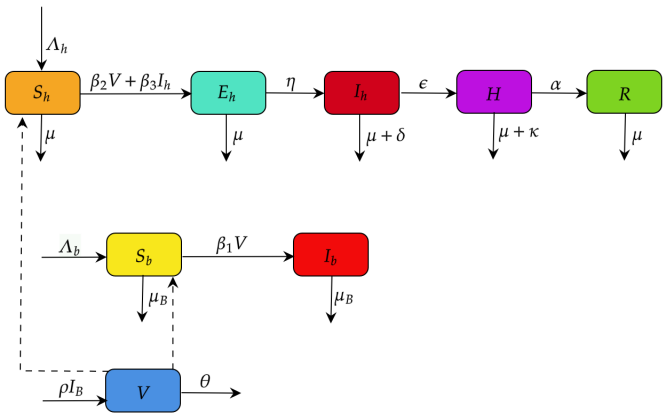

Figure 3: Schematic diagram of the proposed model.

3. The mathematical analysis of the system

3.1. *Positivity and boundedness of the solution*

From the model system (2.1), we have

$$\left.\frac{dV}{dt}\right|_{V=0} = \rho I_b \geqslant 0, \quad \left.\frac{dS_b}{dt}\right|_{S_b=0} = \Lambda_b > 0, \quad \left.\frac{dI_b}{dt}\right|_{I_b=0} = \beta_1 V S_b \geqslant 0, \quad \left.\frac{dS_h}{dt}\right|_{S_h=0} = \Lambda_h > 0,$$
$$\left.\frac{dE_h}{dt}\right|_{E_H=0} = (\beta_2 V + \beta_3 I_h) S_h \geqslant 0, \quad \left.\frac{dI_h}{dt}\right|_{I_h=0} = \eta E_h \geqslant 0, \quad \left.\frac{dH}{dt}\right|_{H=0} = \epsilon I_h \geqslant 0, \quad \left.\frac{dR}{dt}\right|_{R=0} = \alpha H \geqslant 0.$$

Here, all the rates are non-negative on the bounding planes. So, if we start in the interior of the non-negative bounded cone R^8_+, we will remain in this cone. The vector field direction is inward on all the bounding planes. Therefore, the solution to equation (2.1) will always be non-negative. Furthermore, from the model (2.1), we conclude that the total population of humans and bats, N_b and N_h, satisfy

$$\frac{dN_b}{dt} = \Lambda_b - \mu_b S_b - \mu_b I_b = \Lambda_b - \mu_b N_b,$$

and

$$\begin{aligned}\frac{dN_h}{dt} &= \Lambda_h - \mu S_h - \mu E_h - \mu I_h - \mu H - \mu R - \delta I_h - \kappa H,\\ &\leqslant \Lambda_h - \mu S_h - \mu E_h - \mu I_h - \mu H - \mu R = \Lambda_h - \mu N_h.\end{aligned}$$

This gives $\lim_{t\to\infty} \sup N_b \leqslant \frac{\Lambda_b}{\mu_b}$ and $\lim_{t\to\infty} \sup N_h \leqslant \frac{\Lambda_h}{\mu}$. Therefore, every solution S_b and I_b is bounded by $\frac{\Lambda_b}{\mu_b}$ and every solution S_h, E_h, I_h, H, and R is bounded by $\frac{\Lambda_h}{\mu}$. This gives us the biologically feasible region of the system (2.1) by the below positively invariant set

$$\Omega = \left\{(S_b, I_b, S_h, E_h, H, R) : S_b + I_b \leqslant \frac{\Lambda_b}{\mu_b}, S_h + E_h + I_h + H + R \leqslant \frac{\Lambda_h}{\mu}\right\}.$$

3.2. The basic reproduction number

The disease-free equilibrium is given by

$$E_0 = (V^0, S_b^0, I_b^0, S_h^0, E_h^0, I_h^0, H^0, R^0) = (0, \frac{\Lambda_b}{\mu_b}, 0, \frac{\Lambda_h}{\mu}, 0, 0, 0, 0).$$

The Basic Reproduction Number (R_0), evaluates the average number of new NiV cases produced by one typical infectious individual amidst a susceptible population. We applying the Next Generation Matrix Method, elucidated in a study by [13, 19, 37]. To determine the basic reproduction number R_0, we calculate the matrices $\mathcal{F}$ and $\mathcal{V}$ for our model in the following manner

$$\mathcal{F} = \begin{pmatrix} 0 \\ \beta_1 V S_b \\ (\beta_2 V + \beta_3 I_H) S_h \\ 0 \end{pmatrix} \quad \text{and} \quad \mathcal{V} = \begin{pmatrix} -\rho I_b + \theta V \\ (\mu_b I_b) \\ (\eta + \mu) E_h \\ -\eta E_h + (\delta + \mu + \epsilon) I_h \end{pmatrix},$$

$$F = \text{Jacobian of } \mathcal{F} \text{ at } E_0 = \begin{pmatrix} 0 & 0 & 0 & 0 \\ \frac{\beta_1 \Lambda_b}{\mu_b} & 0 & 0 & 0 \\ \frac{\beta_2 \Lambda_h}{\mu} & 0 & 0 & \frac{\beta_3 \Lambda_h}{\mu} \\ 0 & 0 & 0 & 0 \end{pmatrix},$$

and

$$V = \text{Jacobian of } \mathcal{V} \text{ at } E_0 = \begin{pmatrix} \theta & -\rho & 0 & 0 \\ 0 & \mu_b & 0 & 0 \\ 0 & 0 & \eta + \mu & 0 \\ 0 & 0 & -\eta & \delta + \mu + \epsilon \end{pmatrix}.$$

The spectral radius of the matrix FV^{-1} gives the basic reproduction number R_0 and is given by

$$R_0 = \max\left\{\frac{\beta_1 \Lambda_b \rho}{\mu_b^2 \theta}, \frac{\beta_3 \Lambda_h \eta}{\mu(\eta + \mu)(\delta + \epsilon + \mu)}\right\}.$$

3.3. Equilibria

3.3.1. Disease-free equlibrium

Theorem 3.1. *The disease-free equilibrium (DFE) is given by*

$$E_0 = (V^0, S_b^0, I_b^0, S_h^0, E_h^0, I_h^0, H^0, R^0) = \left(0, \frac{\Lambda_b}{\mu_b}, 0, \frac{\Lambda_h}{\mu}, 0, 0, 0, 0\right)$$

and is locally asymptotically stable if $A_3 > 0$, $A_4 > 0$, $A_1A_2A_3 > A_3^2 + A_1^2A_4$, *and is unstable otherwise. Here, the expressions* A_1, A_2, A_3, *and* A_4 *are given in the proof of the theorem.*

Proof. The Jacobian matrix of the model system (2.1) evaluated at the disease-free equilibrium point E_0 is given by

$$J = \begin{pmatrix} -\theta & 0 & \rho & 0 & 0 & 0 & 0 & 0 \\ -\beta_1 S_b^0 & -(\beta_1 V^0 + \mu_b) & 0 & 0 & 0 & 0 & 0 & 0 \\ \beta_1 S_b^0 & \beta_1 V^0 & -\mu_b & 0 & 0 & 0 & 0 & 0 \\ -\beta_2 S_h^0 & 0 & 0 & -(A+\mu) & 0 & -\beta_3 S_h^0 & 0 & 0 \\ \beta_2 S_h^0 & 0 & 0 & A & -(\eta+\mu) & \beta_3 S_h^0 & 0 & 0 \\ 0 & 0 & 0 & 0 & \eta & -B & 0 & 0 \\ 0 & 0 & 0 & 0 & 0 & \epsilon & -C & 0 \\ 0 & 0 & 0 & 0 & 0 & 0 & \alpha & -\mu \end{pmatrix},$$

where $A = (\beta_2 V^0 + \beta_3 I_h^0)$, $B = (\delta + \mu + \epsilon)$, and $C = (\alpha + \mu + \kappa)$. The characteristic equation of J is

$$(\lambda+\mu)^2(\lambda+\mu_b)(\lambda+C)(\lambda^4 + A_1\lambda^3 + A_2\lambda^2 + A_3\lambda + A_4) = 0, \tag{3.1}$$

where

$$\begin{aligned} A_1 &= (a + b + \mu_b + \theta), \\ A_2 &= \frac{ab\mu - \eta\beta_3\Lambda_h + (a+b)\mu_b\mu + (a+b+\mu_b)\theta\mu}{\mu} - \frac{\rho\beta_1\Lambda_b}{\mu_b}, \\ A_3 &= \frac{ab\mu\mu_b - \eta\beta_3\Lambda_h\mu_b + ab\theta\mu - \eta\theta\beta_3\Lambda_h + (a+b)\theta\mu_b\mu}{\mu} - \frac{\rho\beta_1\Lambda_b}{\mu_b}(a+b), \\ A_4 &= \frac{ab\theta\mu\mu_b - \eta\beta_3\theta\Lambda_h\mu_b}{\mu} - \frac{\rho\beta_1\Lambda}{\mu_b}\left(\frac{ab\mu - \eta\beta_3\Lambda_h}{\mu}\right), \end{aligned}$$

with $a = (\eta + \mu)$, $b = (\delta + \mu + \epsilon)$. Clearly, -$\mu$, -$\mu$, -$\mu_b$, and -C are negative real roots of (3.1). By using Routh-Hurwitz Criteria, the remaining roots of the above equation (3.1) will have negative real parts if

$$A_1 > 0, \quad A_3 > 0, \quad A_4 > 0, \quad A_1A_2A_3 > A_3^2 + A_1^2A_4.$$

Here, $A_1 > 0$, so E_0 is locally asymptotically stable if the other three inequalities mentioned above are satisfied. □

3.3.2. Endemic equilibrium

Theorem 3.2. *The endemic equilibrium given by* $E_1 = (V^*, S_b^*, I_b^*, S_h^*, E_h^*, I_h^*, H^*, R^*)$ *for the model described by the system of equation* (2.1) *exists only when* $R_0 > 1$.

Proof. The endemic equilibrium point has the following components:

$$S_b^* = \frac{\Lambda_b}{\beta_1 V^* + \mu_b}, \qquad V^* = \frac{\rho I_b^*}{\theta}, \qquad I_b^* = \frac{\Lambda_b\beta_1\rho - \theta\mu_b^2}{\beta_1\rho\mu_b},$$

$$S_h^* = \frac{\Lambda_h}{\beta_2 V^* + \beta_3 I_h^* + \mu}, \qquad I_h^* = \frac{\eta E_h^*}{\delta + \epsilon + \mu}, \qquad H^* = \frac{\epsilon I_h^*}{\alpha + \mu + \kappa}, \qquad R^* = \frac{\alpha H^*}{\mu},$$

$$E_h^* = \frac{\left(\frac{\beta_2 \rho I_b^*}{\theta} + \frac{\beta_3 \eta E_h^*}{\delta+\epsilon+\mu}\right)\left(\frac{\Lambda_h}{\frac{\beta_2 \rho I_b^*}{\theta} + \frac{\beta_3 \eta E_h^*}{\delta+\epsilon+\mu} + \mu}\right)}{\eta + \mu}, \quad A_1 E_h^2 + A_2 E_h - A_3 = 0,$$

where

$$\begin{aligned}
A_1 &= \beta_3 \eta \theta \eta + \mu, \\
A_2 &= (\eta + \mu \frac{\Lambda_b \beta_1 \rho - \theta \mu_b^2}{\beta_1 \rho \mu_b} (\delta + \epsilon + \mu) \beta_2 \rho + \eta + \mu (\delta + \epsilon + \mu) \mu \theta (1 - R_0)), \\
A_3 &= \beta_2 \rho \Lambda_h \frac{\Lambda_b \beta_1 \rho - \theta \mu_b^2}{\beta_1 \rho \mu_b} (\delta + \epsilon + \mu).
\end{aligned}$$

The roots of the quadratic equation are $\frac{-A_2 + \sqrt{A_2{}^2 + 4A_1A_3}}{2A_1}$ and $\frac{-A_2 - \sqrt{A_2{}^2 + 4A_1A_3}}{2A_1}$. Here $A_1 > 0$ and $A_2^2 + 4A_1A_3 > 0$ so there exists a unique positive root as $E^* = \frac{-A_2 + \sqrt{A_2{}^2 + 4A_1A_3}}{2A_1}$. □

Theorem 3.3. *The endemic equilibrium is locally asymptotically stable if* $B_3 > 0$, $B_1B_2 > B_3$, *and* $B_6 > 0$, $B_4B_5 > B_6$, *and otherwise unstable. Here, the expressions* B_1, B_2, B_3, B_4, B_5, *and* B_6 *are given in the proof of the theorem.*

Proof.

$$J = \begin{pmatrix}
-\theta & 0 & \rho & 0 & 0 & 0 & 0 & 0 \\
-\beta_1 S_b^* & -(\beta_1 V^* + \mu_b) & 0 & 0 & 0 & 0 & 0 & 0 \\
\beta_1 S_b^* & \beta_1 V^* & -\mu_b & 0 & 0 & 0 & 0 & 0 \\
-\beta_2 S_h^* & 0 & 0 & -(A + \mu) & 0 & -\beta_3 S_h^* & 0 & 0 \\
\beta_2 S_h^* & 0 & 0 & A & -(\eta + \mu) & \beta_3 S_h^* & 0 & 0 \\
0 & 0 & 0 & 0 & \eta & -B & 0 & 0 \\
0 & 0 & 0 & 0 & 0 & \epsilon & -C & 0 \\
0 & 0 & 0 & 0 & 0 & 0 & \alpha & -\mu
\end{pmatrix},$$

where $A = (\beta_2 V^* + \beta_3 I_h^*)$, $B = (\delta + \mu + \epsilon)$, and $C = (\alpha + \mu + \kappa)$. The above characteristic polynomial is

$$(\lambda + \mu)(\lambda + C)(\lambda^3 + B_1\lambda^2 + B_2\lambda + B_3)(\lambda^3 + B_4\lambda^2 + B_5\lambda + B_6) = 0, \tag{3.2}$$

with

$$\begin{aligned}
B_1 &= -(a_{11} + a_{22} + a_{33}), & B_2 &= a_{11}a_{22} + a_{11}a_{33} + a_{22}a_{33} - a_{13}a_{31}, \\
B_3 &= -(a_{11}a_{22}a_{33} + a_{13}a_{21}a_{32} - a_{13}a_{31}a_{22}), & B_4 &= -(a_{44} + a_{55} + a_{66}), \\
B_5 &= a_{44}a_{55} + a_{44}a_{66} + a_{55}a_{66}, & B_6 &= -(a_{44}a_{55}a_{66} + a_{46}a_{54} - a_{65}a_{56}).
\end{aligned}$$

Here, $a_{11} = -\theta$, $a_{13} = \rho$, $a_{21} = -\beta_1 S_b^*$, $a_{22} = -(\beta_1 V^* + \mu_b)$, $a_{31} = \beta_1 S_b^*$, $a_{32} = \beta_1 V^*$, $a_{33} = -\mu_b$, $a_{44} = -((\beta_2 V^* + \beta_3 I_h^*) + \mu)$, $a_{46} = -\beta_3 S_h^*$, $a_{54} = (\beta_2 V^* + \beta_3 I_h^*)$, $a_{55} = -(\eta + \mu)$, $a_{56} = \beta_3 S_h^*$, $a_{65} = \eta$, $a_{66} = -(\delta + \mu + \epsilon)$. Clearly, $-\mu$ and $-C$ are negative real roots of (3.2). By using Routh-Hurwitz criteria, the remaining roots of the equation (3.2) will have negative real parts provided $B_1 > 0$, $B_3 > 0$, $B_1B_2 > B_3$, and $B_4 > 0$, $B_6 > 0$, $B_4B_5 > B_6$. Clearly, $B_1 > 0$ and $B_4 > 0$, so the equilibrium point E_1 is locally asymptotically stable if other four conditions mentioned above are satisfied. □

4. Numerical simulation

In this section, Nipah virus data from Bangladesh have been fitted, and the impact of key parameters on Nipah virus prevalence has been analyzed.

Table 1: Fitted parameter values.

Parameters	Values	95% confidence interval	References
ρ	0.02306	0.02093 - 0.02519	Fitted
θ	0.87177	0.80769 - 0.93586	Fitted
β_1	0.00511	0.00149 - 0.00971	Fitted
β_2	0.06701	0.06434 - 0.06968	Fitted
β_3	0.40381	0.37706 - 0.43056	Fitted
η	0.98682	0.96823 - 1.00542	Fitted
ϵ	0.74494	0.70647 - 0.78342	Fitted
α	0.50358	0.42587 - 0.58128	Fitted

Table 2: Parameter values.

Parameters	Values	References
Λ_h	1816348	Calculated
Λ_b	300	[34]
δ	0.7096	Calculated
κ	0.71	Assumed
μ	1/74 = 0.0135	Calculated
μ_b	0.04	Calculated

4.1. Data fitting

The proposed model demonstrates that parameter estimation using the Nipah Virus Disease data of Bangladesh by maximum likelihood estimation (MLE) is a robust method for the proposed model. The model parameters that best suit the observed data can be determined by optimizing a function that indicates how well the model fits the data. Here, the unit of all parameters is in year$^-$1. We estimated ten model parameters using Python programming to capture the complexities of Nipah virus dynamics. These parameters include transmission, recovery, progression, hospitalization, virus shedding, and decay rates. We fitted our model to the cumulative number of infected cases using data from Bangladesh covering the period from 2010 to 2023, [40]. The estimated parameters, along with the remaining parameters, are detailed in Tables 1 and 2, respectively. The parameter δ represents the disease-related death rate for the infected human compartment, calculated as Total Death Cases / Total Confirmed Cases $= \frac{242}{341}$ = 0.7096 [6]. Additionally, the parameter Λ_h denotes the recruitment rate for the human population of Bangladesh in 2010, which can be computed using the total population multiplied by the natural death rate: 134544296 * 0.0135 = 1816348 [6]. The data fitting for the proposed model is illustrated in Figure 4.

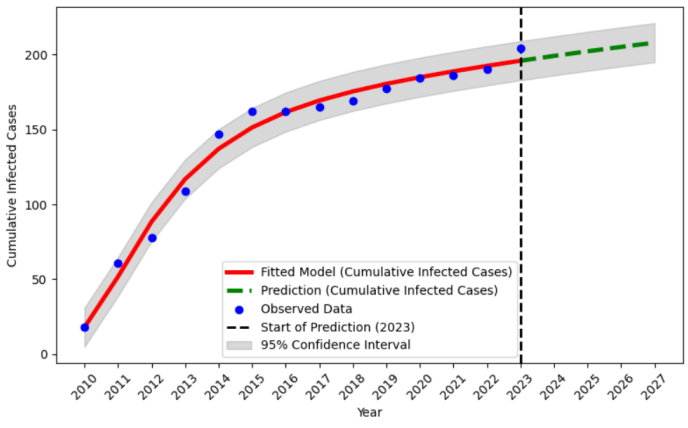

Figure 4: Graph illustrating the fitted model showcasing Nipah virus yearly cumulative cases in Bangladesh from 2010 to 2026. The red curve illustrates the model solution, the dotted green line shows the prediction, and the blue dots depict the real data.

4.2. Sensitivity analysis

Here we perform sensitivity analysis to study the effect of the model parameters on the basic reproduction number $R_0 = \max\left\{\frac{\beta_1\Lambda_b\rho}{\mu_b^2\theta}, \frac{\beta_3\Lambda_h\eta}{\mu(\eta+\mu)(\delta+\epsilon+\mu)}\right\}$. According to the parameter values presented in Table 1, it has been observed that $\frac{\beta_1\Lambda_b\rho}{\mu_b^2\theta} < \frac{\beta_3\Lambda_h\eta}{\mu(\eta+\mu)(\delta+\epsilon+\mu)}$. Consequently, we can infer that $R_0 = \frac{\beta_3\Lambda_h\eta}{\mu(\eta+\mu)(\delta+\epsilon+\mu)}$. This analysis reveals that changes in the parameter directly affect R_0 it can be an increase or decrease in R_0. The normalized forward sensitivity index for a parameter compares how the parameter's relative change corresponds to the relative change in the R_0 [11]. If the variable is a differentiable function of the parameter, an alternative definition for the sensitivity index can be established using partial derivatives. The normalized forward sensitivity index of R_0, contingent upon the differentiability concerning a parameter denoted as 'q', is defined as

$$r_q^{R_0} = \frac{\partial R_0}{\partial q} \times \frac{q}{R_0}.$$

By utilizing this formula, we have determined the sensitivity indices R_0 and depicted them in Figure 5.

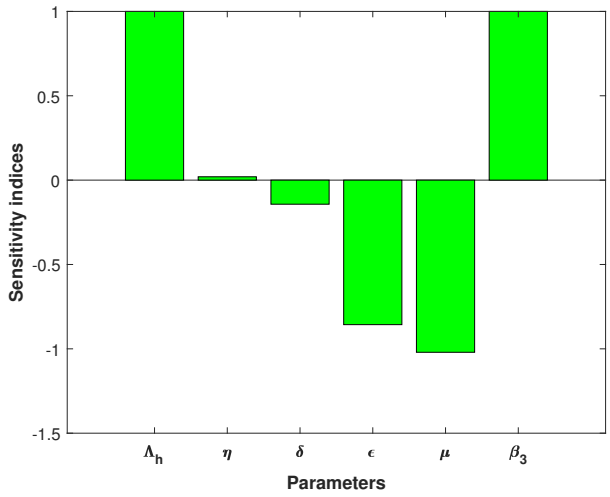

Figure 5: The normalized forward sensitivity index of the basic reproduction number (R_0).

From this figure we observed that Λ_h, η, and β_3 have a positive impact on R_0, whereas δ, ϵ, and μ have a negative impact. This indicates that the number of secondary infections increases as the recruitment rate of humans (Λ_h), progression rate of infection state (η), and disease transmission rate (β_3) increase, while it decreases when the disease-related death rate (δ), hospitalization rate (ϵ), and natural death rate (μ) increase.

Analyzing the simultaneous comparison of two parameters and their impact on the basic reproduction number R_0 is a fundamental aspect of sensitivity analysis and modeling in epidemiology and various scientific fields. Here Figure 6a depicts the variations of the basic reproduction number R_0. As the transmission rate β_3 increases, so does the value of R_0, indicating a greater spread of the disease. Conversely, when the hospitalization rate ϵ increases, the transmission rate decreases, resulting in a reduction in disease spread, and this result is shown in 3-D Figure 6b.

Figure 7a illustrates that an increase in the infection rate β_3 leads to a rise in the value of the basic reproduction number R_0 as well as the migration parameter from the exposed class to the infected class, denoted as η. Figure 7a implies that controlling or increasing this component can aid in decreasing the spread of illness. Similarly to the preceding part, a 3-D figure is displayed in Figure 7b. This method enables researchers to comprehend the interplay and impact of several factors on the transmission of diseases.

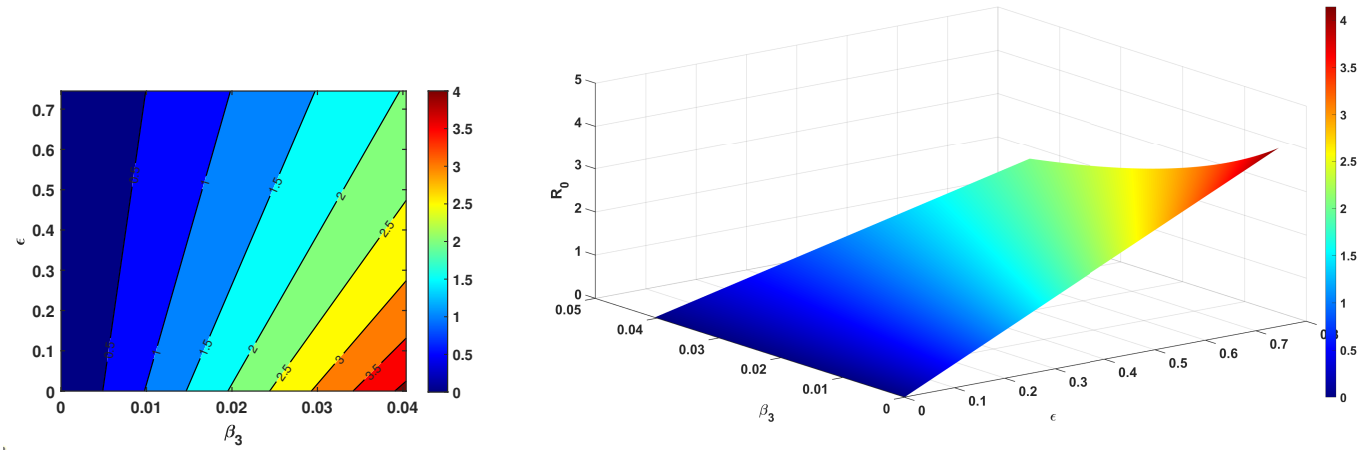

(a) **(b)**

Figure 6: Sensitivity of the basic reproduction number (R_0) with respect to the parameter β_3, ϵ.

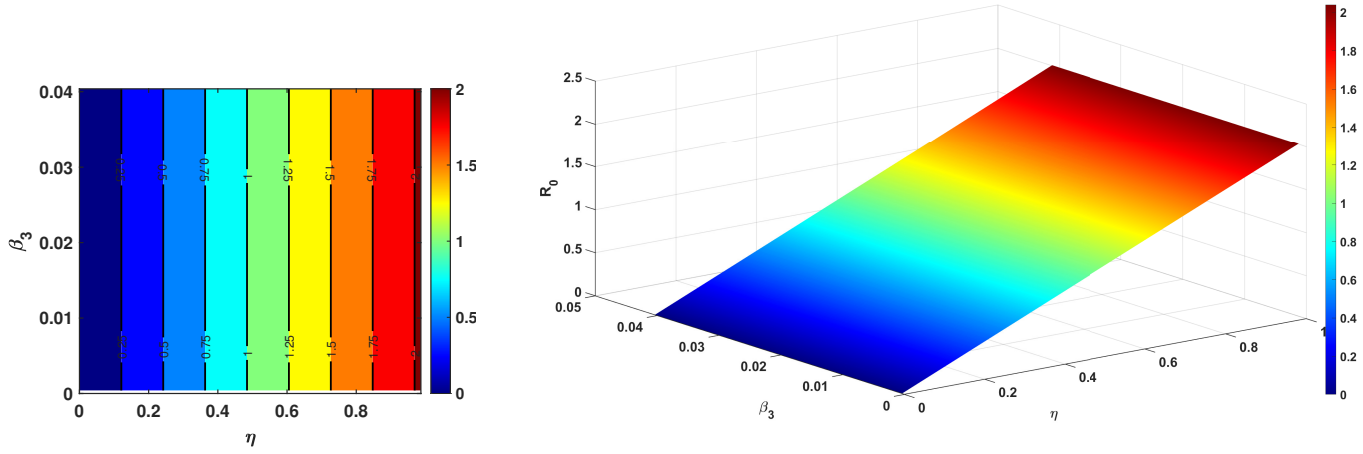

(a) **(b)**

Figure 7: Sensitivity of the basic reproduction number (R_0) with respect to the parameter β_3, η.

4.3. Impact of parameters on transmission of Nipah virus

Here, we investigate the model (2.1) time-series dynamics. It concerns Virus V and recovered R concerning the model's parameters. Studying the system's behavior by changing parameter values one at a time and observing the effect on the system is a helpful technique for understanding how the model system works and how to control its dynamics.

Figure 8a illustrates the impact of ρ in a virus population. The virus compartment has a more significant infection with an increase in the shedding rate ρ. Figure 8b illustrates the rise in the recovered rate α, resulting in a more number of recoveries.

Figure 9 demonstrates that an increase in the hospitalization rate (ϵ) leads to a decrease in the number of infected individuals (I_h), while simultaneously increasing the number of hospitalized individuals (H) and those who have recovered (R). This trend is depicted in Figures 9a, 9b, and 9c. The observed changes can be attributed to more effective treatment, reducing the spread of the disease. Overall, the dynamics suggest that as more infected individuals are hospitalized, the healthcare system is better equipped to treat them, leading to higher recovery rates and reduced disease transmission. This supports the importance of early detection and proper medical care in managing infectious diseases [18].

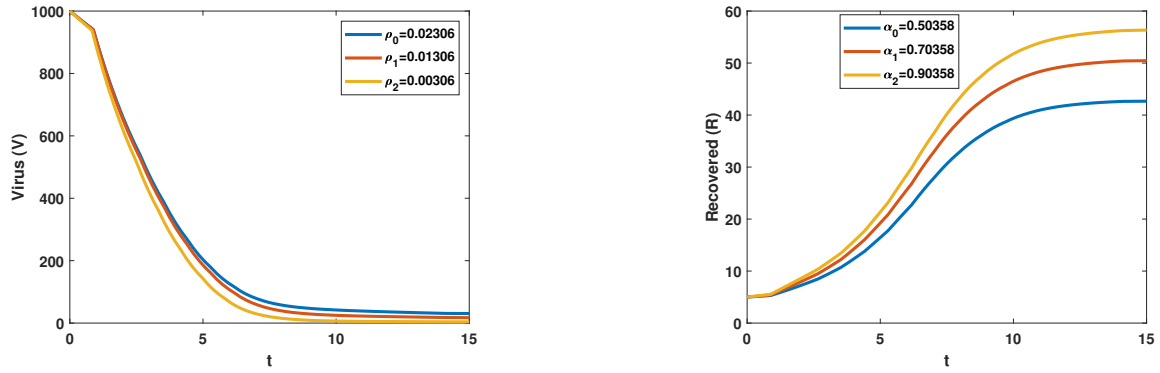

(a) (b)

Figure 8: Time series of model (2.1) illustrating variations in (a) virus population over time for different values of the parameter ρ and (b) recovered individuals over time for different values of the parameter α.

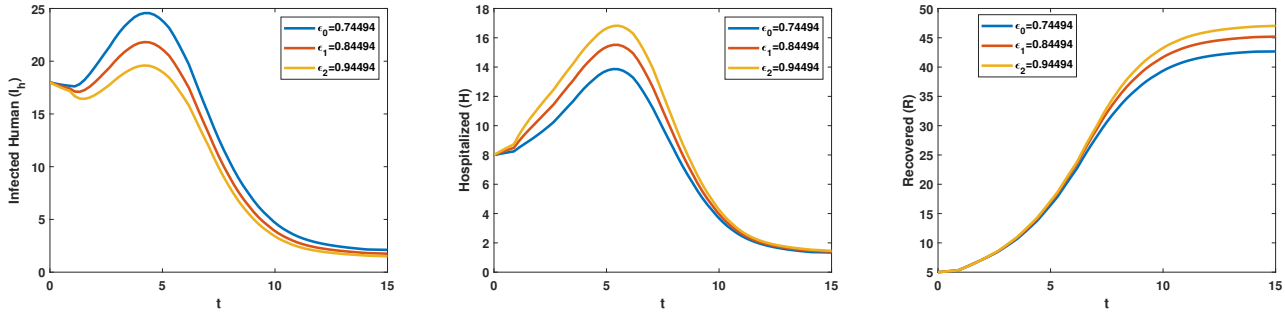

(a) (b) (c)

Figure 9: Time series of model (2.1) depict the variation in (a) infected individuals, (b) hospitalized individuals, and (c) recovered individuals over time for various values of the ϵ parameters.

5. Optimal control

Optimal control is an invaluable mathematical tool that may be employed to control the propagation of infection within a population. The primary objective of this research is to identify the most effective control strategies that can be implemented with minimal cost. In numerous epidemiological problems, optimal control has been demonstrated to be a successful approach. In this section, we expand the mathematical model outlined in Eqs. (5.1) by introducing control parameters to formulate an optimal control problem with three control parameters, denoted as u_1 u_2 and u_3 associated with the culling rate of the bat population, reduce the transmission and enhance treatment, respectively.

The culling of bat population as a control measure was incorporated in the mathematical model discussed in [21]. Similarly, the culling of the pig population is implemented in controlling the outbreak of this disease in Malaysia, where more than 1 million pigs were culled, which led to a reduction in the total infected cases [23]. This type of control was incorporated in the mathematical model investigated in [42]. Here, the control variable u_1 indicates the culling rate of the bat population, which aims to minimize the spread of the virus by decreasing the number of infected individuals.

The control parameter u_2 plays a crucial that directly reduces the transmission rate. It can be conceptualized as a proactive measure akin to enforcing the mandatory washing of fruits before eating [9, 20, 33]. These measures collectively minimize the spread of infections and enhance public health safety.

The control parameter u_3, which concentrates on hospitalization and testing centers, can be highly beneficial in identifying and controlling the spread of disease [17]. Adopting a comprehensive approach to disease control necessitates incorporating all three measures u_1, u_2, and u_3. While u_1 emphasizes controlling the bat population through culling, u_2 aims to curb transmission from human to human, and u_3 focuses on preventing and treating infections in affected individuals. Collectively, these three control

parameters play a vital role in controlling and managing the spread of the disease.

$$\begin{aligned}
\frac{dV}{dt} &= \rho I_b - \theta V,\\
\frac{dS_b}{dt} &= \Lambda_b + \beta_1 V S_b - (\mu_b + u_1(t))S_b,\\
\frac{dI_b}{dt} &= \beta_1 V S_b - (\mu_b + u_1(t))I_b,\\
\frac{dS_h}{dt} &= \Lambda_h - (1-u_2(t))(\beta_2 V + \beta_3 I_h)S_h - \mu S_h,\\
\frac{dE_h}{dt} &= (1-u_2(t))(\beta_2 V + \beta_3 I_h)S_h - (\eta+\mu)E_h,\\
\frac{dI_h}{dt} &= \eta E_h - (\delta + \mu + u_3(t) + \epsilon)I_h,\\
\frac{dH}{dt} &= (\epsilon + u_3(t))I_h - (\mu + \kappa + \alpha)H,\\
\frac{dR}{dt} &= \alpha H - \mu R.
\end{aligned} \tag{5.1}$$

The objective function for the fixed time t_f is given by

$$J = \int_0^{t_f} (C_1 V + C_2 I_b + C_3 I_h + C_4 H + \frac{1}{2}C_5 u_1^2 + \frac{1}{2}C_6 u_2^2 + \frac{1}{2}C_7 u_3^2)dt,$$

where $C_1, C_2, C_3, C_4, C_5, C_6, C_7 \geqslant 0$ are seven weight constants. The objective is to ascertain the control parameters u_1^*, u_2^*, u_3^*, such that $J(u_1^*, u_2^*, u_3^*) = \min\ J(u_1, u_2, u_3)$. Here, Ω_1 is the defined control set. $\Omega_1 = \{u_1, u_2, u_3$: measurable and $0 \leqslant u_1, u_2, u_3 < 1\}$ and t belongs to $[0, t_f]$. The Lagrangian of this problem is:

$$L(V, I_b, I_h, H, u_1, u_2, u_3) = C_1 V + C_2 I_b + C_3 I_h + C_4 H + \frac{1}{2}C_5 u_1^2 + \frac{1}{2}C_6 u_2^2 + \frac{1}{2}C_7 u_3^2.$$

The Hamiltonian $\mathcal{H}$ formulated for our problem is

$$\mathcal{H} = L(V, I_b, I_h, H, u_1, u_2, u_3) + \lambda_1 \frac{dV}{dt} + \lambda_2 \frac{dS_b}{dt} + \lambda_3 \frac{dI_b}{dt} + \lambda_4 \frac{dS_h}{dt} + \lambda_5 \frac{dI_h}{dt} + \lambda_6 \frac{dE_h}{dt} + \lambda_7 \frac{dH}{dt} + \lambda_8 \frac{dR}{dt},$$

where λ_i's represents the adjoint variables for $i = 1, \ldots, 8$. The results from Fleming and Rishel [15] assure that an optimal control problem exists. The adjoint variables are represented in the form of differential equations as follows:

$$\begin{aligned}
\frac{d\lambda_1}{dt} &= -\frac{\partial \mathcal{H}}{\partial V} = \lambda_1 \phi + \beta_1 S_b(\lambda_2 - \lambda_3) + \beta_2 S_h(\lambda_4 - \lambda_5)(1-u_2(t)) - C_1,\\
\frac{d\lambda_2}{dt} &= -\frac{\partial \mathcal{H}}{\partial S_b} = \beta_1 V(\lambda_2 - \lambda_3) + (\mu_b + u_1(t))\lambda_2,\\
\frac{d\lambda_3}{dt} &= -\frac{\partial \mathcal{H}}{\partial I_b} = (\mu_b + u_1(t))\lambda_3 - \rho\lambda_3 - C_2,\\
\frac{d\lambda_4}{dt} &= -\frac{\partial \mathcal{H}}{\partial S_h} = (1-u_2(t))(\beta_2 V + \beta_3 I_h)(\lambda_4 - \lambda_5) + \mu\lambda_4,\\
\frac{d\lambda_5}{dt} &= -\frac{\partial \mathcal{H}}{\partial E_h} = \eta(\lambda_5 - \lambda_6) + \mu\lambda_5,\\
\frac{d\lambda_6}{dt} &= -\frac{\partial \mathcal{H}}{\partial I_h} = (\epsilon + u_3(t))(\lambda_6 - \lambda_7) + (\mu + \delta)\lambda_6 + (1-u_2(t))\beta_3 S_h(\lambda_4 - \lambda_5) - C_3,\\
\frac{d\lambda_7}{dt} &= -\frac{\partial \mathcal{H}}{\partial H} = \alpha(\lambda_7 - \lambda_8) + (\mu + \kappa)\lambda_7 - C_4,
\end{aligned}$$

$$\frac{d\lambda_8}{dt} = -\frac{\partial \mathcal{H}}{\partial R} = \mu\lambda_8.$$

Let $\tilde{V}$, $\tilde{S_b}$, $\tilde{I_b}$, $\tilde{S_h}$, $\tilde{I_h}$, $\tilde{E_h}$, $\tilde{H}$ and $\tilde{R}$ be the optimal values of V, S_b, I_b, S_h, E_h, I_h, H and R, respectively. Let $\tilde{\lambda_1}$, $\tilde{\lambda_2}$, $\tilde{\lambda_3}$, $\tilde{\lambda_4}$, $\tilde{\lambda_5}$, $\tilde{\lambda_6}$, $\tilde{\lambda_7}$, and $\tilde{\lambda_8}$ be solutions of (5.1), we present and demonstrate the following theorem.

Theorem 5.1. *Optimal controls u_1^*, u_2^*, u_3^* belonging to set Ω_1 exist, such that $J(u_1^*, u_2^*, u_3^*) = \min J(u_1, u_2, u_3)$ subject to the extended system of equations (5.1).*

Proof. We utilize [30] to establish this theorem. In this scenario, it is evident that the controls are non-negative. The necessary convexity of the objective function in (u_1, u_2, u_3) is satisfied for the minimization problem. A set of control variables such as u_1, u_2, and u_3 within Ω_1 is both convex and closed by definition. The state variables are bounded, and the integral is functional $C_1V + C_2I_b + C_3I_h + C_4H + \frac{1}{2}C_5u_1^2 + \frac{1}{2}C_6u_2^2 + \frac{1}{2}C_7u_3^2$ and is convex on Ω_1.

As optimal controls exist for minimizing the functional subject to systems (2.1) and (5.1), we employ Pontryagin's maximum principle to derive the necessary conditions for finding the optimal solutions in the following manner. Suppose (z, u) is an optimal solution of an optimal control problem, then, this implies the existence of a non-trivial vector function $\lambda = \lambda_1, \lambda_2, \ldots, \lambda_n$ satisfying the following:

$$\frac{dz}{dt} = \frac{\partial \mathcal{H}(t, z, u, \lambda)}{\partial \lambda}, \quad 0 = \frac{\partial \mathcal{H}(t, z, u, \lambda)}{\partial u}, \quad \frac{d\lambda}{dt} = \frac{\partial \mathcal{H}(t, z, u, \lambda)}{\partial z}.$$

□

Theorem 5.2. *The optimal controls u_1^*, u_2^*, u_3^* that minimize J over the region Ω_1 are expressed as:*

$$u_1^* = \min\left\{1, \max(0, \tilde{u_1})\right\}, \quad u_2^* = \min\left\{1, \max(0, \tilde{u_2})\right\}, \quad u_3^* = \min\left\{1, \max(0, \tilde{u_3})\right\},$$

where,

$$\tilde{u}_1 = \frac{\lambda_2 S_b + \lambda_3 I_b}{C_5}, \quad \tilde{u}_2 = \frac{(\beta_2 V + \beta_3 I_h)(\lambda_5 - \lambda_4) S_h}{C_6}, \quad \tilde{u}_3 = \frac{(\lambda_6 - \lambda_7) I_h}{C_7}.$$

Proof. We establish this theorem by utilizing [30] and Theorem 5.1. Applying the optimality condition: $\frac{\partial \mathcal{H}}{\partial u_1} = 0$, $\frac{\partial \mathcal{H}}{\partial u_2} = 0$, $\frac{\partial \mathcal{H}}{\partial u_3} = 0$, we get

$$\begin{aligned}
&\frac{\partial \mathcal{H}}{\partial u_1} = C_5u_1 - \lambda_2 S_b - \lambda_3 I_b = 0 \quad \Longrightarrow \quad u_1 = \frac{\lambda_2 S_b + \lambda_3 I_b}{C_5} = \tilde{u}_1, \\
&\frac{\partial \mathcal{H}}{\partial u_2} = C_6u_2 + (\beta_2 V + \beta_3 I_h)(\lambda_4 - \lambda_5) S_h = 0 \quad \Longrightarrow \quad u_2 = \frac{(\beta_2 V + \beta_3 I_h)(\lambda_5 - \lambda_4) S_h}{C_6} = \tilde{u}_2, \\
&\frac{\partial \mathcal{H}}{\partial u_3} = C_7u_3 + (\lambda_7 - \lambda_6) I_h = 0 \quad \Longrightarrow \quad u_3 = \frac{(\lambda_6 - \lambda_7) I_h}{C_7} = \tilde{u}_3.
\end{aligned}$$

The controls u_1, u_2, u_3 have a lower bound of 0 and an upper bound of 1. This suggests that $u_1 = u_2 = u_3 = 0$ if $\tilde{u}_1 < 0$, $\tilde{u}_2 < 0$, and $\tilde{u}_3 < 0$, also $u_1 = u_2 = u_3 = 1$ if $\tilde{u}_1 > 1$, $\tilde{u}_2 > 1$, and $\tilde{u}_3 > 1$, other wise $u_1 = \tilde{u}_1$, $u_2 = \tilde{u}_2$, $u_3 = \tilde{u}_3$. Hence, for these controls u_1^*, u_2^*, u_3^*, we obtain optimal values for J. □

5.1. Simulation of optimal control problem

The optimal control problem is simulated using MATLAB for 150 days. The weight constants are $C_1 = 1, C_2 = 1, C_3 = 1, C_4 = 1, C_5 = 15, C_6 = 40$, and $C_7 = 55$. The extended system of equations (5.1) is iteratively solved using forward and backward difference approximations [24]. Figure 10 shows the control profiles of u_1, u_2, and u_3 for apply all three control. These figures indicate that the control profile u_2 should be sustained at 1 for an extended period compared to the other control. This control is associated with reducing disease transmission through mandatory washing of fruits before eating. Adherence to these measures by the entire population can significantly diminish the spread of the disease. In the following subsections, we are focusing on the impact of different control strategies.

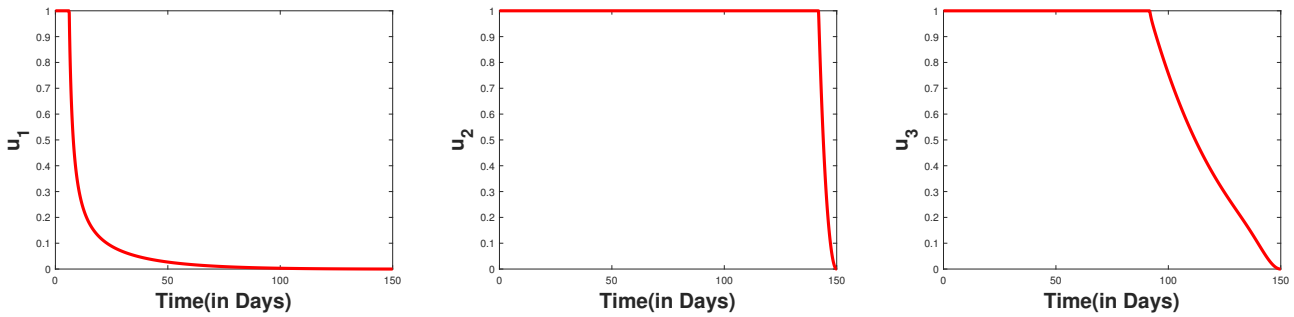

(a) (b) (c)

Figure 10: Control profile of (a) u_1; (b) u_2; and (c) u_3.

5.1.1. Strategy A: culling of bats (u_1) only

The analysis specifically focuses on the control parameter u_1, which pertains to the culling of the bat population. In contrast, other control variables, such as measures to reduce transmission rate and hospitalization (u_2 and u_3), are set to zero. Figure 11 illustrates the impact of control measures on the infected human population.

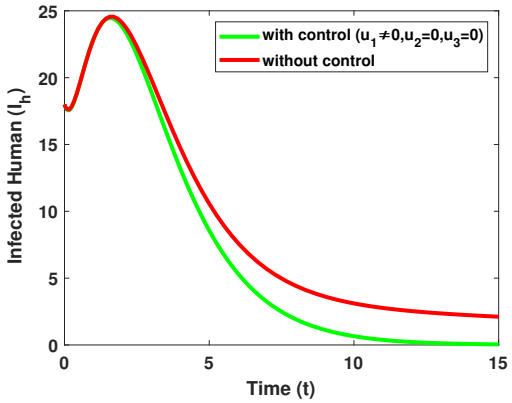

Figure 11: Variations of infected human (I_h) with and without control for u_1 only.

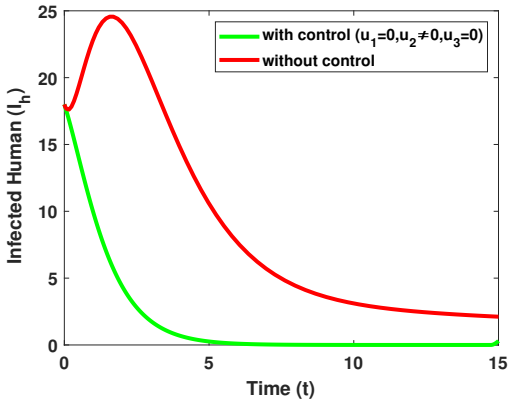

Figure 12: Variations of infected human (I_h) with and without control for u_2 only.

5.1.2. Strategy B: reducing the transmission (u_2) only

Strategy B involves implementing measures to reduce the transmission rates, such as practicing good hygiene, ensuring food safety, and increasing usage of sanitizers. In contrast, the culling of bat-related and hospitalization-related controls (u_1 and u_3) are all set to zero. Figure 12 shows the impact of control measures u_2 on the infected population, specifically focusing on the implementation of only one control measure (u_2).

5.1.3. Strategy C: increasing hospitalization (u_3) only

Strategy C consists of providing enhanced treatment and care, which may involve prompt medical intervention and effective isolation protocols. Only control u_3 is implemented, other two controls are set to zero. Figure 13 illustrate the impact of these control measures on the infected population.

5.1.4. Strategy D: culling bats and reducing transmission u_1 and u_2

Strategy D shows the effect of implementing two control measures u_1 and u_2 simultaneously, namely culling the animal population and reducing the human transmission rate in the infected population. Here, hospitalization control u_3 is set to zero in this strategy. Figure 14 shows the impact of both u_1 and u_2 control measures on the infected population.

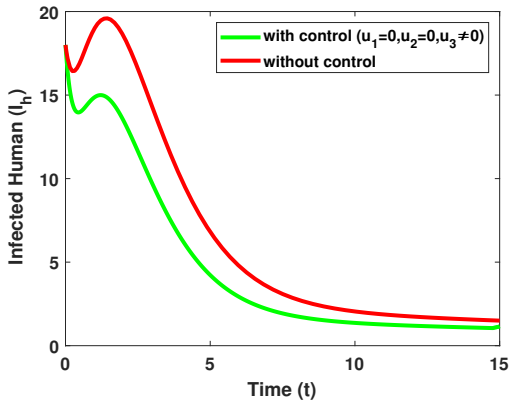

Figure 13: Variations of infected human (I_h) with and without control for u_3 only.

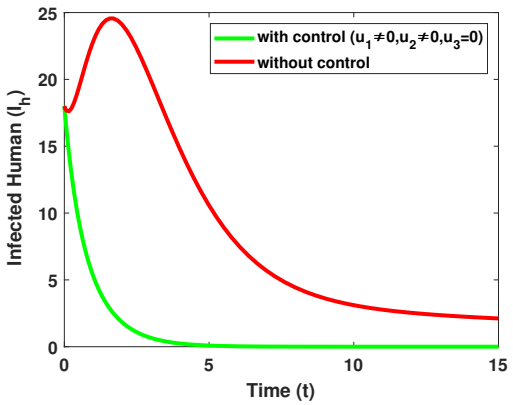

Figure 14: Variations of infected human (I_h) with and without control for u_1 and u_2.

5.1.5. *Strategy E: reducing transmission and hospitalization* u_2 *and* u_3

Strategy E presents the cumulative effect of implementing two concurrent control measures, denoted as u_2 and u_3, which involve reducing human transmission and hospitalizations, respectively, in the infected population, as depicted in Figure 15. By concurrently employing both control strategies, it is possible to effectively curb disease transmission within the population.

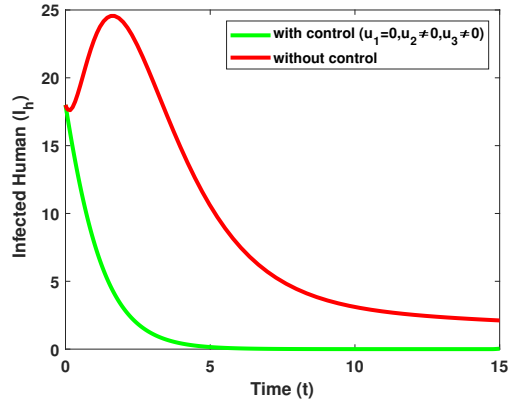

Figure 15: Variations of infected human (I_h) with and without control for u_2 and u_3.

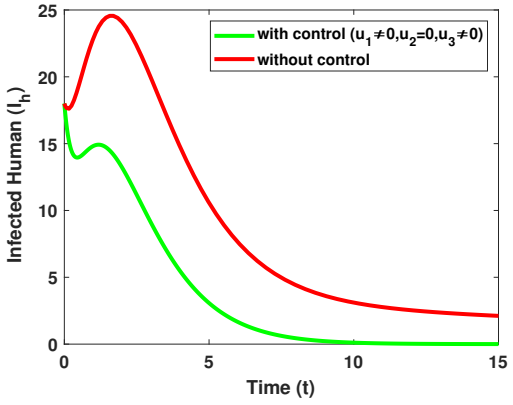

Figure 16: Variations of infected human (I_h) with and without control for u_1 and u_3.

5.1.6. *Strategy F: culling bats and hospitalization* u_1 *and* u_3

Strategy F includes both the culling rate of an animal population u_1 and hospitalization u_3 control for the infected population, this can be illustrated in the Figure 16.

5.1.7. *Strategy G: culling bats, reducing transmission, and hospitalization* u_1, u_2, *and* u_3

Strategy G represents the integration of all control measures implemented collectively. We've included here the simulation results of strategy G compared to the absence of control measures. Figure 17 indicates that strategy G is highly effective in controlling the number of Nipah-infected individuals and recovered individuals. The simulation result reveals a significant decline in the number of infected individuals across all population categories when all three control measures are implemented simultaneously. This observation highlights the efficacy of the optimal control strategy in reducing infection rates within the specified time frame. Moreover, a substantial reduction in the total counts of infected individual is evident upon the simultaneous execution of all three control measures, as depicted in Figure 17.

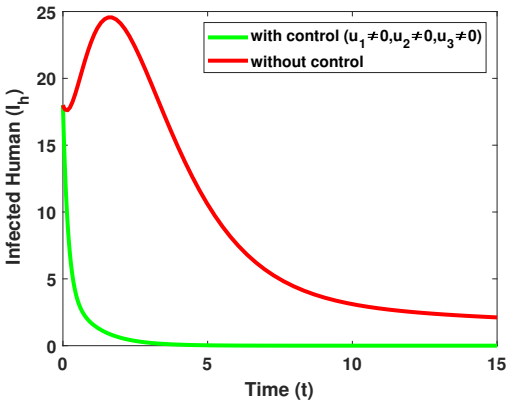

Figure 17: Variations of infected human (I_h) with and without control for u_1, u_2, and u_2.

5.2. Cost-effectiveness analysis

In this section, we analyze and evaluate the economic viability and epidemiological impact of the proposed intervention strategies. A cost-effectiveness analysis was performed using the outcomes of the optimal control model for Nipah virus transmission. Within this framework, various control strategies-such as bat culling (u_1), reduction of human-to-human transmission (u_2), and enhanced hospitalization or treatment (u_3)-were implemented both individually and in combination. The effectiveness of each strategy was assessed by calculating the total cost of the intervention and the total number of infections averted over the simulation period. These metrics were then used to determine the Incremental Cost-Effectiveness Ratio (ICER), allowing for comparisons of the strategies against a no-control baseline and against one another. This approach provides a quantitative basis for identifying the most economically efficient control policy aimed at minimizing the spread of the Nipah virus. Average cost-effectiveness ratio (ACER) is usually expressed by

$$ACER = \frac{\text{Total cost associated with implementing a specific intervention strategy}}{\text{Total number of infections prevented by the intervention strategy}}.$$

The ICER is defined as the quotient of the difference in costs in strategies i and j, by the difference in infected averted in strategies i and j ($i, j \in \{1-7\}$) [12, 22, 38]. Given two competing strategies, (1) and (2), where strategy (2) demonstrates higher effectiveness than strategy (1) (TA(2) $>$ TA(1)), the ICER values are calculated as follows:

$$ICER(1) = \frac{TC(1)}{TA(1)}, \quad ICER(2) = \frac{TC(2) - TC(1)}{TA(2) - TA(1)},$$

where the total cost (TC) and total cases averted (TA) are defined as

$$TC = \frac{1}{2}\int_0^{t_f} \sum_{i=1}^{3} C_i u_i^2 dt.$$

The total contagions averted (TA) is calculated by taking the difference between the number of Nipah virus contagions that occur with the strategy and the number of contagions that occur without the strategy.

To determine the final ICER values, a stepwise comparison is conducted across all strategies. Any strategy that incurs a higher cost while providing fewer or equal benefits is considered dominated and excluded from further analysis. The remaining strategies are then compared sequentially in order of increasing effectiveness. The ICER values derived from this process help identify the most cost-effective strategy, serving as a rational basis for optimal resource allocation in public health interventions.

Figure 18 and Table 3 show that Strategy 7 has the highest ACER values, while Strategy 1 has the lowest. A lower ACER indicates better cost-effectiveness, meaning fewer costs are incurred per infection

averted. Furthermore, the analysis was extended to calculate the Incremental Cost-Effectiveness Ratio (ICER) values for all seven strategies. In Table 3, Strategy 7 demonstrates the lowest cost-effectiveness compared to the other strategies, leading to its elimination from further consideration. Subsequently, we continue the process by removing additional less cost-effective strategies. Finally, in Table 7, we present Strategy 1 as the most cost-effective option. Therefore, Strategy 1 is identified as the most cost-effective among the seven strategies evaluated in this study.

Table 3: ICER (incremental cost-effectiveness ratio).

Strategy	Infection averted	Total cost	ACER	ICER
Strategy 1	27.1314	48.7343	1.7962	1.7962
Strategy 3	65.1096	339.9134	5.2206	7.667
Strategy 5	79.8812	442.0473	5.5338	6.9142
Strategy 2	110.6762	296.8457	2.6821	-4.7151
Strategy 4	110.6798	341.0844	3.0817	12288.52
Strategy 6	121.0785	294.4500	2.4318	-4.4846
Strategy 7	121.0934	774.9262	6.3994	32246.72

Table 4: ICER (incremental cost-effectiveness ratio).

Strategy	Infection averted	Total cost	ACER	ICER
Strategy 1	27.1314	48.7343	1.7962	1.7962
Strategy 3	65.1096	339.9134	5.2206	7.667
Strategy 5	79.8812	442.0473	5.5338	6.9142
Strategy 2	110.6762	296.8457	2.6821	-4.7151
Strategy 4	110.6798	341.0844	3.0817	12288.52
Strategy 6	121.0785	294.4500	2.4318	-4.4846

Table 5: ICER (incremental cost-effectiveness ratio).

Strategy	Infection averted	cost	ACER	ICER
Strategy 1	27.1314	48.7343	1.7962	1.7962
Strategy 3	65.1096	339.9134	5.2206	7.667
Strategy 5	79.8812	442.0473	5.5338	6.9142
Strategy 2	110.6762	296.8457	2.6821	-4.7151
Strategy 6	121.0785	294.4500	2.4318	-0.2298

Table 6: ICER (incremental cost-effectiveness ratio).

Strategy	Infection averted	Total cost	ACER	ICER
Strategy 1	27.1314	48.7343	1.7962	1.7962
Strategy 5	79.8812	442.0473	5.5338	7.4561
Strategy 2	110.6762	296.8457	2.6821	-4.7151
Strategy 6	121.0785	294.4500	2.4318	-0.2298

Table 7: ICER (incremental cost-effectiveness ratio).

Strategy	Infection averted	Total cost	ACER	ICER
Strategy 1	27.1314	48.7343	1.7962	1.7962
Strategy 2	110.6762	296.8457	2.6821	2.9698
Strategy 6	121.0785	294.4500	2.4318	-0.2303

Table 8: ICER (incremental cost-effectiveness ratio).

Strategy	Infection averted	Total cost	ACER	ICER
Strategy 1	27.1314	48.7343	1.7962	1.7962
Strategy 6	121.0785	294.4500	2.4318	2.6154

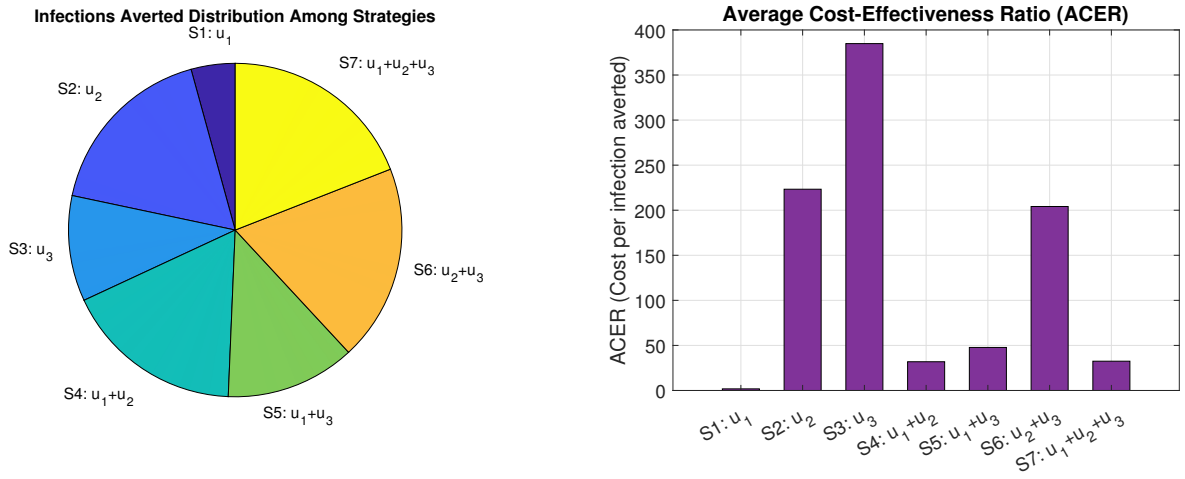

(a) **(b)**

Figure 18: (a) Pie chart showing the proportion of total infections averted by each of the seven control strategies. Strategy 7 (u_1, u_2, u_3) exhibits the largest share, indicating its strong effectiveness. (b) Bar diagram of Average Cost-Effectiveness Ratio (ACER), where a lower ACER implies a more cost-effective strategy. Strategy 1 (u_1) offers the lowest ACER value, highlighting their efficiency in resource utilization.

6. Conclusion

The present paper proposed a mathematical framework for analyzing the transmission dynamics of the Nipah virus. We developed an eight-compartment model to describe the interactions between virus, bats and humans. At the time of the study, no vaccine was available to prevent Nipah virus infection, and the only available treatment was supportive care. We investigated the impact of increases hospitalization rates in reducing the transmission of the Nipah virus and performed numerical simulations to validate our model. Our fundamental analysis focused on the model's reproduction number, equilibria, and stability. We also examined a normalized sensitivity analysis to identify the most sensitive parameter and determine the effective optimal control. The optimal control strategies identified involve culling the bat population (u_1), reducing transmission between the human population (u_2), and increasing hospitalization and testing centers (u_3). Among these, only one control strategy, strategy B reducing the transmission control measure, was found to be more effective in decreasing the number of infections than the other two control strategies, namely strategy A and strategy C. Our simulations showed that implementing all of these controls led to reduction in the peak infection rate.

A cost-effectiveness analysis using both ACER and ICER metrics was also carried out to evaluate the economic feasibility of each strategy. While Strategy 7 (all controls combined) achieved the highest reduction in infections, it was not the most cost-efficient. Strategy 1, involving only bat population control, demonstrated the lowest cost per infection averted and was ultimately identified as the most cost-effective approach. These findings suggest that a focused, resource-conscious control strategy can yield substantial epidemiological impact.

In future work, we plan to study the mobility and age factors, which are essential in the transmission of infectious diseases.

Data availability

The data supporting this study are publicly available at the WHO website: https://www.who.int/emergencies/disease-outbreak-news/item/2024-DON508.

Declaration of competing interest

The authors declare that they have no competing financial interests or personal relationships that could have appeared to influence the work reported in this paper.

Acknowledgment

The authors are grateful to the anonymous referees for their valuable suggestions, which improved the manuscript and presentation. This research was supported by internal support from Vellore Institute of Technology, Chennai, India. First author is supported by VIT Research Fellowship.

References

[1] P. Agarwal, R. Singh, *Modelling of transmission dynamics of Nipah virus (Niv): a fractional order approach*, Phys. A, **547** (2020), 11 pages. 1, 1
[2] A. Ahmad, F. Abbas, M. Farman, E. Hincal, A. Ghaffar, A. Akgül, M. K. Hassani, *Flip bifurcation analysis and mathematical modeling of cholera disease by taking control measures*, Sci. Rep., **14** (2024), 31 pages. 1
[3] A. Ahmad, S. Abbas, M. Inc, A. Ghaffar, *Stability analysis of SARS-CoV-2 with heart attack effected patients and bifurcation*, Adv. Biol., **8** (2024). 1
[4] A. Ahmad, M. Farman, P. A. Naik, K. Faiz, A. Ghaffar, E. Hincal, M. U. Saleem, *Analytical analysis and bifurcation of pine wilt dynamical transmission with host vector and nonlinear incidence using sustainable fractional approach*, Partial Differ. Equ. Appl. Math., **11** (2024), 26 pages. 1
[5] A. Ahmad, Q. M. Farooq, H. Ahmad, D. Uzun Ozsahin, F. Tchier, A. Ghaffar, G. Mustafa, *Study on symptomatic and asymptomatic transmissions of COVID-19 including flip bifurcation*, Int. J. Biomath., **18** (2025), 34 pages. 1
[6] N. I. Akinwande, S. A. Somma, R. O. Olayiwola, T. T. Ashezua, R. I. Gweryina, F. A. Oguntolu, O. N. Abdurahman, F. S. Kaduna, T. P. Adajime, F. A. Kuta, S. Abdulrahman, A. I. Enagi, G. A. Bolarin, M. D. Shehu, A. Usman, *Modelling the impacts of media campaign and double dose vaccination in controlling COVID-19 in Nigeria*, Alex. Eng. J., **80** (2023), 167–190. 4.1
[7] D. Baleanu, P. Shekari, L. Torkzadeh, H. Ranjbar, A. Jajarmi, K. Nouri, *Stability analysis and system properties of Nipah virus transmission: a fractional calculus case study*, Chaos Solitons Fractals, **166** (2023), 10 pages. 1
[8] S. Barua, A. Dénes, *Global dynamics of a compartmental model for the spread of Nipah virus*, Heliyon, **9** (2023), 15 pages. 1
[9] S. Bhattacharyya, S. K. Kumar, S. Majumdar, M. Dutta, *Nipah virus infections*, Clin. Nursing, **2** (2023), 4 pages. 5
[10] Centers for Disease Control and Prevention, *Nipah virus: About*, (accessed 2025). 1
[11] N. Chitnis, J. M. Hyman, J. M. Cushing, *Determining important parameters in the spread of malaria through the sensitivity analysis of a mathematical model*, Bull. Math. Biol., **70** (2008), 1272–1296. 4.2
[12] Y. Deng, Y. Zhao, *Mathematical modeling for COVID-19 with focus on intervention strategies and cost-effectiveness analysis*, Nonlinear Dyn., **110** (2022), 3893–3919. 5.2
[13] O. Diekmann, J. A. P. Heesterbeek, J. A. J. Metz, *On the definition and the computation of the basic reproduction ratio* R_0 *in models for infectious diseases in heterogeneous populations*, J. Math. Biol., **28** (1990), 365–382. 3.2
[14] F. Evirgen, *Transmission of Nipah virus dynamics under Caputo fractional derivative*, J. Comput. Appl. Math., **418** (2023), 16 pages. 1
[15] W. H. Fleming, R. W. Rishel, *Deterministic and stochastic optimal control*, Springer-Verlag, Berlin-New York, (1975). 5
[16] N. K. Goswami, F. Hategekimana, *Optimal control techniques for the transmission risk of Nipah virus disease with awareness*, Adv. Syst. Sci. Appl., **22** (2022), 176–192. 1
[17] M. Z. Hassan, A. Rojek, P. Olliaro, P. Horby, *Improving clinical care of patients in Nipah outbreaks: moving beyond 'compassionate use'*, Lancet Reg. Health Southeast Asia, **33** (2025), 5 pages. 5
[18] M. Z. Hassan, H. M. S. Sazzad, S. P. Luby, K. Sturm-Ramirez, M. U. Bhuiyan, M. Z. Rahman, M. M. Islam, U. Ströher, S. Sultana, M. A. H. Kafi, P. Daszak, M. Rahman, E. S. Gurley, *Nipah virus contamination of hospital surfaces during outbreaks, Bangladesh, 2013–2014*, Emerg. Infect. Dis., **24** (2018), 15–21. 4.3
[19] H. W. Hethcote, *The mathematics of infectious diseases*, SIAM Rev., **42** (2000), 599–653. 3.2
[20] J. M. Hughes, M. E. Wilson, S. P. Luby, E. S. Gurley, M. J. Hossain, *Transmission of human infection with Nipah virus*, Clin. Infect. Dis., **49** (2009), 1743–1748. 5

[21] M. Y. Khan, S. Ullah, M. Farooq, B. Al Alwan, A. B. Saqib, *Optimal control analysis for the Nipah infection with constant and time-varying vaccination and treatment under real data application*, Sci. Rep., **14** (2024), 25 pages. 1, 5
[22] A. Kouidere, O. Balatif, M. Rachik, *Cost-effectiveness of a mathematical modeling with optimal control approach of spread of COVID-19 pandemic: A case study in Peru*, Chaos Solitons Fractals X, **10** (2023), 11 pages. 5.2
[23] S. K. Lam, K. B. Chua, *Nipah virus encephalitis outbreak in Malaysia*, Clin. Infect. Dis., **34** (2002), S48–S51. 5
[24] S. Lenhart, J. T. Workman, *Optimal control applied to biological models*, Chapman & Hall/CRC, Boca Raton, FL, (2007). 5.1
[25] M. Mabotsa, J. M. J. Munganga, *Mathematical modelling of the spread of Nipah virus in bats, humans and pigs*, J. Interdiscip. Math., **28** (2025), 1453–1488. 1
[26] A. Malek, N. Islam, A. Hoque,*Investigations of transmission dynamics of Nipah virus in Bangladesh*, Inform. Med. Unlocked., **44** (2024), 9 pages. 1
[27] M. K. Mondal, M. Hanif, M. H. A. Biswas, *A mathematical analysis for controlling the spread of Nipah virus infection*, Int. J. Model. Simul., **37** (2017), 185–197. 1
[28] B. I. Omede, P. O. Ameh, A. Omame, B. Bolaji, *Modelling the transmission dynamics of Nipah virus with optimal control*, arXiv preprint arXiv:2010.04111, (2020), 29 pages. 1
[29] P. Panja, R. K. Jana, *Optimal control of a Nipah virus transmission model*, In: Mathematical Modeling and Soft Computing in Epidemiology, CRC Press, (2020), 127–146. 1
[30] L. S. Pontryagin, *Mathematical theory of optimal processes*, Routledge, London, (2018). 5, 5
[31] Samreen, S. Ullah, R. Nawaz, S. A. AlQahtani, S. Li, A. M. Hassan, *A mathematical study unfolding the transmission and control of deadly Nipah virus infection under optimized preventive measures: New insights using fractional calculus*, Results Phys., **51** (2023), 28 pages. 1
[32] N. H. Shah, A. H. Suthar, F. A. Thakkar, M. H. Satia, *SEI-model for transmission of Nipah virus*, J. Math. Comput. Sci., **8** (2018), 714–730. 1
[33] R. K. Singh, K. Dhama, S. Chakraborty, R. Tiwari, S. Natesan, R. Khandia, A. Munjal, K. S. Vora, S. K. Latheef, K. Karthik, Y. S. Malik, R. Singh, W. Chaicumpa, D. T. Mourya, *Nipah virus: epidemiology, pathology, immunobiology and advances in diagnosis, vaccine designing and control strategies-a comprehensive review*, Vet. Q., **39** (2019), 26–55. 5
[34] D. Sinha, A. Sinha, *Mathematical model of zoonotic Nipah virus in South-East Asia region*, Acta Sci. Microbiol., **2** (2019), 82–89. 1, 2
[35] J. Sultana, C. N. Podder, *Mathematical analysis of Nipah virus infections using optimal control theory*, J. Appl. Math. Phys., **4** (2016), 1099–1111. 1
[36] P. K. Uppal, *Emergence of Nipah virus in Malaysia*, Ann. N. Y. Acad. Sci., **916** (2000), 354–357. 1
[37] P. Van den Driessche, J. Watmough, *Reproduction numbers and sub-threshold endemic equilibria for compartmental models of disease transmission*, Math. Biosci., **180** (2002), 29–48. 3.2
[38] A. Venkatesh, M. A. Rao, *Mathematical model for COVID-19 pandemic with implementation of intervention strategies and cost-effectiveness analysis*, Results Control Optim., **14** (2024), 18 pages. 5.2
[39] World Health Organization, *Nipah virus infection*, (accessed 2025). 1
[40] World Health Organization, *Disease Outbreak News: 2023-DON442*, available at: `https://www.who.int/emergencies/disease-outbreak-news/item/2023-DON442` (accessed 2025). 1, 4.1
[41] A. D. Zewdie, S. Gakkhar, *A mathematical model for Nipah virus infection*, J. Appl. Math., **2020** (2020), 10 pages. 1
[42] A. D. Zewdie, S. Gakkhar, S. K. Gupta, *Human-animal Nipah virus transmission: model analysis and optimal control*, Int. J. Dyn. Control, **11** (2023), 1974–1994. 1, 5